Cooperating Parties Group

LOWER PASSAIC RIVER RI/FS
NEWARK, NEW JERSEY

APPENDIX M - ATTACHMENT F

SETTLING VELOCITY ANALYSIS

Prepared by:



F.1 Introduction

The settling velocity of sediment in suspension is an important parameter in modeling the transport and fate of fine sediments in the natural environment. The settling velocity of sand particles can be estimated as a quadratic function of the grain size. The relationship of the settling velocity of cohesive sediments to their grain size however is complicated by the tendency of cohesive particles to form of porous flocs. The settling velocity of cohesive sediments has therefore to be estimated on the basis of literature data, or measured directly using sophisticated instruments such as the floc camera. However, a direct measurement of settling velocity can seldom be used as input to numerical modeling, as calibration of that model depends on other parameters as well.

As an alternative to field measurements of settling velocity, data on measured suspended sediments and flow velocities in the water column can be used to estimate the bulk settling velocity. In comparison to most field measurements of settling velocity which are typically limited in their spatial and temporal extent, a major advantage of this approach is that it is based on a large dataset of suspended sediment measurements and therefore less sensitive to local anomalies in space and time. In this analysis, data on measured vertical suspended sediment concentrations (SSC) and flow velocities was used to estimate the cohesive settling velocity. Moreover, this method uses the measured vertical gradients in SSC, which are also subject of model evaluation.

The following sections present the theoretical background of this method, and the results for the Lower Passaic River. The relevance of the settling velocity estimates and their use in the modeling is also discussed.

F.2 Theoretical Background

The vertical distribution of SSC is described by the mass balance equation, which uses information on flow velocity and turbulent mixing. These equations are resolved numerically within ECOM-SEDZLJS. These equations can also be used to establish the settling velocity based on observations of vertical SSC distributions with the following assumptions:

- The velocity distribution over the water depth is logarithmic, which is the case if:
    - the water column is neutrally buoyant, i.e. no vertical gradients in salinity or SSC that affect vertical mixing,
    - flow accelerations and decelerations are small
- The water column shear stress profile is a linear function of depth. In combination with the preceding assumption, this results in a parabolic eddy viscosity profile.
- The horizontal gradients (in main flow direction) in SSC are small.

- Vertical gradients in SSC are governed by a local equilibrium between vertical turbulent mixing and the sediment's settling velocity.

Then the vertical SSC distribution follows Rouse distribution (e.g. Van Rijn, 1984):

$$\frac{C}{C_a} = \left[\frac{a\left(1-\frac{z}{h}\right)}{z\left(1-\frac{a}{h}\right)}\right]^{\beta} \quad (1)$$

where,

$$\beta = \frac{\sigma_T W_S}{\kappa u_*} \quad (2)$$

C = SSC measured at level z (z = 0 at riverbed),

C_a = SSC at reference height a,

h = the total water depth,

β = the so-called Rouse number,

W_S = bulk settling velocity,

σ_T = turbulent Prandtl-Schmidt number ($\sigma_T \approx 0.7$),

κ = Von Karman constant ($\kappa = 0.41$), and

u_* = shear velocity.

It should be noted that because the suspended particles are not homogeneous, but are characterized by a particle size distribution, they follow a corresponding settling velocity distribution. As the SSC data represent a bulk sediment composition, the Rouse profile can only represent mean values, and the computed settling velocity W_S should be regarded as a representative measure of the entire settling velocity distribution, similar to the median settling velocity.

To obtain the bulk settling velocity from the measured SSC distribution, first the Rouse number β is established from the measured SSC values by fitting Equation 1 to the observations. It is assumed that 10-12 minute SSC values will give reasonably accurate results. The shear velocity is calculated from the flow velocity measured in the bottom bin of the ADCP ensemble using the formulation used in ECOM-SEDZLJS:

$$u_* = \frac{\kappa u}{log\left(\frac{z}{z_0}\right)} \quad (3)$$

where,

$$z_0 = \frac{2d_{eff}}{30} \quad (4)$$

u = velocity in the ADCP bottom bin (m/s),

z = mid-point of ADCP bottom bin from bed (m),

z_0 = grain roughness factor (m), and

d_{eff} = effective diameter of sediment in bed (m).

Equation 1 is fit to the data by means of a least-squares optimization function. The resulting Rouse number is used to calculate the settling velocity using the shear velocity and grain roughness height calculated using Equations 3 and 4.

It is also important to note a couple of differences between the Rouse profile formulation and the ECOM-SEDZLJS numerical model used for the numerical modeling in LPRSA. As mentioned previously, the Rouse profile assumes a parabolic eddy viscosity profile; however, within the numerical model the viscosity profile is calculated by the turbulence closure scheme and can deviate from the parabolic profile. In addition, the Rouse profile approach relates the turbulent eddy viscosity to the eddy diffusivity (used for the vertical mixing of suspended sediments and other scalars) by means of the turbulent Prandtl-Schmidt number (σ_T = 0.7); for ECOM-SEDZLJS application to the LPRSA, the eddy diffusivity is set to the same value as eddy viscosity. Both these differences imply certain limitations in directly applying the results of this analysis to the model. Nonetheless, the analysis does provide information on the bulk settling velocity (within the context of the Rouse profile formulation) that informs the system understanding of sediment transport, can guide the development of the model, and also serves as a starting point for the model calibration efforts.

F.3 Analysis and Results

The following datasets were used in the analysis of settling velocities:

- Data collected as part of the Physical Water Column Monitoring (PWCM) program during October to December 2009, with five ADCP moorings deployed at RMs 1.4, 4.2, 6.7, 10.2 and 13.5, measuring at 12 minute frequency

- Time-series of ADCP data collected by Sommerfield and Chant (2010) in the LPR at RM 1.4 from September 2008 to March 2009, with measurements every 10 minutes

Both these datasets provide estimates of suspended sediment concentrations from acoustic backscatter measurements, as well as flow velocities, measured over a number of bins through the water column.

The results of the settling velocity analysis are shown in Figure 1 through Figure 23. In these figures the results of the Fall 2009 PWCM data for RMs 1.4, 4.2, 6.7, 10.2 and 13.5 are shown, as well as the RM 1.4 data by Chant.

Figure 1 through Figure 3 show some characteristic vertical SSC profiles, together with the Rouse fits through the data. As these profiles and fits were made every 10-12 minutes, it is not possible to present all results. In general, the Rouse fits match the SSC data quite well, but there are some exceptions. In particular, near the water surface at RM 1.4, the SSC data show some anomalous behavior, with increasing SSC values in the upper part of the water column. These anomalies were found in particular in the lower miles of the river; Figure 3, data for RM 13.5, do not show this behavior. Similarly, the data from the bottom-most bin also occasionally shows lower SSC values than the next bin above as seen for several of the profiles in Figure 2. Therefore, the data from the bottom-most bin and the surface-most bin measured by the ADCP were excluded at all times for the characterization of the vertical SSC profile, due to such spurious data trends, likely due to artifacts such as surface reflections and blanking issues (at the bottom of the water column; similar artifacts have been reported by other authors such as Wall et al, 2006). The reversing trends in the upper part of the water column and at the bottom of the profile is therefore assumed to be erroneous, and ignored in this analysis.

Figure 1 through Figure 3 also show the values for near-surface and near-bed salinity measurements and the gradient thereof, the measured near-bed flow velocity, and the computed values for β and W_S, following from the Rouse fits.

Figure 4 through Figure 11 show the time-series of all computed settling velocities, together with the ambient parameters. In the lower miles of the LPR, the settling velocity shows a pronounced correlation with tidal range (also amplitude in flow velocity); such a correlation was also found for the SSC data as well (results not shown here). Furthermore, it is noteworthy that the settling velocities during flood are somewhat larger than during ebb, e.g. Figure 5 and Figure 11. Although the differences between flood and ebb are not very large, they are consistent through time.

Depth-average SSC values within the LPRSA under normal tidal and low-average discharge conditions typically are of the order of 100 mg/l, sometimes somewhat larger, but often even smaller. This implies that flocculation times are so large (days and more; Winterwerp, 2005), that over a tidal cycle, flocculation dynamics do not play a role. However, the cohesive fraction is flocculated, the floc/particle size distribution is constant

over time (tidal cycle), though. Hence, the larger settling velocity during flood implies one of several possibilities:

- larger particles are mobilized with the larger flood velocities, and/or
- larger particles are transported from downstream locations (Newark Bay) into the LPR, with gravitational circulation and tidal asymmetry, and/or
- limitations of the Rouse-approach under stratified conditions, in particular at the beginning of flood when salinity stratification exhibits a maximum (e.g. Figure 5), thus providing a mechanism that dampens vertical mixing of sediments.

Indeed, the tidal signal in W_S, both with respect to the daily variations, as with the spring-neap cycle, disappears further upstream, e.g. Figure 9 and Figure 10.

Figure 12 through Figure 17 show probability distributions of the computed settling velocities, for all data, and all available stations. We have made a distinction between all data, and ebb-data only. This is done because the Rouse-approach fails under stratified conditions, this distinction may yield information on whether this stratification plays a big role. Indeed we observe that the ebb settling velocities in the lower part of the river are a bit smaller than W_S values for all data, whereas this difference becomes almost nil in the upper part of the LPR.

The range in settling velocities is large, varying from around 0.01 mm/s to almost 10 mm/s, i.e. three orders of magnitude. These values are discussed a bit further in a subsequent section. Statistics on the settling velocity at each station were obtained by computing a settling velocity based on each vertical SSC profile in the time-series. Table 1 summarizes the mean and median settling velocities for all stations.

The differences in flood-ebb behavior is further illustrated in Figure 18 through Figure 20, showing that in the lower part of the LPR maximal W_S values on flood are somewhat larger than on ebb. However, at RM 13.5, the ebb-values are the larger, owing to the larger flow velocities during ebb than flood. These figures also show a pronounced positive correlation between settling velocity (floc/particle size) and flow velocity, as discussed above.

Figure 21 through Figure 23 show a very weak correlation between W_S values and SSC-values. Part of this correlation should be directly related to the correlation between W_S and flow velocity discussed previously: at larger flow velocities, not only larger particles are mobilized, but also more particles.

Table 1. Calculated Bulk Settling Velocities in LPR

Location	Grain Size Diameter, d_{eff} (µm)	Calculated Mean W_S (mm/s)	Calculated Median W_S (mm/s)
Sommerfield and Chant's 2008-09 deployment			
LPR, RM 1.4	35.6	2.26	1.43
Fall 2009 PWCM deployment			
LPR, RM 1.4	35.6	2.15	1.47
LPR, RM 4.2	90.5	2.12	0.95
LPR, RM 6.7	76.9	1.56	1.20
LPR, RM 10.2	179.9	1.13	0.93
LPR, RM 13.5	291.7	0.68	0.52

F.4 Discussion

The W_S distribution graphs should be interpreted with care, as they do not represent the physical settling velocity distribution – that information cannot be retrieved from bulk SSC values. The W_S distributions in Figure 12 through Figure 17 merely give an indication on the goodness of fit of the procedure applied. Though the extremes of the computed W_S values differ by three orders of magnitude, the majority of the data lie within a factor of 2 – 5 (± standard deviation around median value).

Under stratified conditions, mixing becomes suppressed, and settling velocities appear larger, as this damping is not accounted for in the Rouse-fits. Indeed, we observe differences for the larger W_S distribution between values based on all data and based on ebb data only in the lower part of the LPR and in Newark Bay, where salinity plays a role.

However, the median value of around 1 mm/s (see below) makes sense, and is in the range of values measured in other rivers and estuaries (Dyer, 1986; Winterwerp and Van Kesteren, 2004).

Time series of W_S correlate well with the daily tidal cycle, and the spring-neap tide cycle. The larger W_S values are found during flood in the lower part of the LPR, whereas in its upper part the larger values are found during ebb. Correlation plots with flow velocity suggest that the higher flow velocities mobilize coarser particles/flocs, whereas the upstream transport of the larger particles is in agreement with observations of larger SSC-values during flood (at low-average river flows).

The data suggest a correlation of W_S with SSC. However, especially at lower range of SSC values (e.g. less than ~10 mg/L in Figure 23), the data are too scattered to allow for a credible algorithm relating W_S and SSC. At higher SSC (e.g. greater than ~10 mg/L in Figure 23), a correlation of increasing W_S with increasing SSC is apparent. However, the reasons for this positive correlation are not entirely clear. One potential explanation may derive from compositional changes at higher flows – for instance, comparing Figures 20 and 23 shows that the data points indicating a positive correlation of W_S with SSC occur at near-bottom ebb velocities greater than ~0.35 m/s, which is very nearly equal to the threshold velocity for resuspension of sands (particle diameters >63 um). This suggests that the suspended sediment at velocities greater than 0.35 m/s may have included some fraction of sand. Since erosion flux scales as a function of shear stress (Van Rijn, 1984), higher velocity implies higher SSC. At the same time, since the threshold for initiation of motion for sand particles scales as a function of particle diameter (Van Rijn, 1984), higher velocity implies larger particles mobilized and in suspension. Similarly, the settling velocity of sand particles also scales as a function of particle diameter (Cheng, 1997). Therefore, one explanation of the apparent correlation in Figure 23 may be due to the W_S-velocity correlation – larger flow velocities mobilize some sand. If true, that implies that sands in suspension may account for the correlation of W_S with SSC noted at SSC greater than ~10 mg/L in Figure 23. Conversely, at the lower end of the SSC range (less than ~10 mg/L in Figure 23), assuming predominantly cohesive sediment composition, implies that there is no relationship between W_S and SSC.

Another possibility that may explain the apparent correlation of W_S with increasing SSC relates to the heterogeneity of cohesive sediments in terms of particle (floc) classes, erosion properties, and also settling velocities. For instance, using data from erosion experiments conducted in annular flume experiments, Van Prooijen and Winterwerp (2010) conceptualized the measured erosion as a combination of various sediment classes associated with varying critical shear stresses for erosion. In other words, at low flow velocities only a subset of sediment classes would be available to erode, with more sediment classes susceptible to erosion with increasing flow velocity. Similarly, LISS-ST data collected in the LPR in the vicinity of the 80 Lister Avenue site (OSI, 2009) show a range of particle (floc) sizes in suspension and with varying settling velocities. Therefore, another explanation of the apparent correlation in Figure 23 may be because higher flow velocities mobilize particle (floc) classes that are more resistant to erosion. It should be noted that although this conceptual picture may be a physically reasonable description of the processes involved, neither the available erosion data in the LPR (neither Sedflume, nor Gust microcosm, nor the entrainment rate analysis), nor the settling velocity analysis presented here, nor the LISS-ST data in the LPR are comprehensive enough to support the development and calibration of a numerical model with multiple cohesive classes.

Therefore, even though some of the W_S data suggest an apparent relation with SSC, the exact reasons behind this phenomenon are not entirely clear. In addition to the above-mentioned complexity and uncertainty in the analysis and interpretation of the W_S data, as mentioned previously in Section F.2, certain assumptions inherent to the Rouse-approach preclude the direct application of the W_S results from this analysis to the ECOM-SEDZLJS

numerical model. Therefore, the results of this analysis have been used to guide the development and parameterization of the numerical model rather than being directly applicable to the numerical model.

The computed W_S values found from the Rouse-fits are also comparable with data obtained during the Pilot Dredging experiment. Figure 24 shows that the sedimentation velocities (e.g. cleansing of the water column) amount to 1 – 1.5 mm/s. These are gross velocities, counteracted by vertical mixing. The effect of vertical mixing can be estimated from a "mixing velocity" V_M, defined as ε_Z/h, where ε_Z = vertical eddy diffusivity and h = water depth. The vertical eddy diffusivity can be estimated from $\varepsilon_Z \approx 0.1hu_*$, which leads to $V_M \approx 0.4$ mm/s. Hence, the sedimentation velocity corrected for the vertical mixing velocity amounts more or less to the W_S values computed from the Rouse fits. This gives further credibility to the results of the analysis.

Figure 25 shows the spatial variation of the median settling velocity from this analysis. Since the majority of the period in both datasets examined in this analysis consisted of flows at or below the long-term average flow at Dundee Dam, the median values are assumed to be indicative of the settling characteristics of cohesive sediments. The spatial trends seen in Figure 25 further contributes to the conclusion on the role of the flow velocity and flood dominated sediment import on particle/floc size, hence settling velocity, showing a consistent decrease in median settling velocity along the LPR. This longitudinal gradient can be explained from longitudinal sorting caused by various processes such as:

- Reduction in net upstream transport of "coarse" material: The net upstream transport of sediments becomes less efficient because of a reduction in asymmetry in tidal currents and in gravitational circulation. Figure 2 and Figure 4 in Appendix M present a quantitative analysis of tidal asymmetry and gravitational circulation at the various stations in the PWCM dataset to illustrate this point. Flood dominance in near-bottom tidal currents is generally seen to be a function of location at given instant, decreasing with distance up-estuary. Near-bottom residual currents are also seen to vary in a similar manner. The decreasing asymmetry in peak tidal currents along with the decrease in tidal currents up-estuary (see the next bullet for a detailed description of this feature), implies decreasing shear stress on average with distance up-estuary during low-average flow conditions. This means a reduction in the mobilization and transport of "coarse" material up-estuary thus providing one mechanism that explains the longitudinal trend in settling velocity

- Reduction in vertical mixing capacity in upstream direction: Figure 4 and Figure 7-10 allow for an assessment of the spatial pattern in tidal currents in the LPR – comparing the peak flood or ebb currents at the various locations in these figures show a general decrease in tidal currents moving up-estuary from RM 1.4 due to a corresponding decrease in the tidal prism. The decrease in vertical mixing due to the decrease in tidal currents with distance up-estuary implies that the "coarser" material (associated with higher settling velocity) will not be retained in

suspension, thus implying only relatively finer material (associated with lower settling velocity) in suspension at the upstream locations.

- Import of poorly-flocculated fine sediments from over Dundee Dam: The suspended sediments in the LPR reflect a combination of sediments entering from Dundee Dam and marine sediments entering from Newark Bay. Due to the role of salinity in promoting flocculation, the marine sediments are expected to be flocculated (Winterwerp and Van Kesteren, 2004). On the other hand, suspended sediments associated with the freshwater inflow from Dundee Dam are expected to be poorly-flocculated. Since flocculation affects the settling velocity of cohesive sediments, amongst other properties, the decrease in median settling velocity with distance up-estuary may also reflect the impact of poorly-flocculated sediments entering from Dundee Dam. Since the tidal prism and therefore available dilution increases with distance down-estuary, the settling velocity signal may become dominated more by marine or flocculated sediments at the down-estuary locations.

F.5 Summary

The application of the Rouse-approach to the various datasets of SSC profiles allows the calculation of bulk settling velocities. These settling velocities have been examined relative to various physical parameters such as the tidal cycle, spring-neap variability, near-bottom velocity, and SSC data. The settling velocity is seen to be a function of the near-bottom velocity, indicating the presence of particles (flocs) with a range of settling velocities in the LPR. The settling velocity results have also been examined for spatial trends and related to tidal and estuarine circulation phenomena. The spatial trends in settling velocity may also indicate the relative influence of suspended sediments from Dundee Dam, which are expected to be poorly-flocculated, versus marine sediments which are expected to be flocculated. These features noted in the data are the basis of the model parameterization selected for the LPR ST model as described in Appendix M.

F.6 References

Cheng, NS, 1997. Simplified Settling Velocity Formula for Sediment Particles, ASCE Journal of Hydraulic Engineering, 123, 149-152.

Dyer, KR, 1986. Coastal and Estuarine Sediment Dynamics. John Wiley & Sons, 342 p.

Ocean Surveys, Inc. (OSI), 2009. Final Report Oceanographic *In Situ* and Real-Time Data Acquisition Program, Passaic River, Newark, NJ. OSI Report No. 09ES045. Prepared for Tierra Solutions, Inc.

Sommerfield, CK, and RJ Chant, 2010. Mechanisms of Sediment Trapping and Accumulation in Newark Bay, New Jersey: An Engineered Estuarine Basin. Final Report to the Hudson River Foundation.

Van Prooijen BC, and JC Winterwerp, 2010. A Stochastic Formulation for Erosion of Cohesive Sediments. J Geophys Res 115, C01005, doi:10.1029/2008JC005189.

van Rijn, LC, 1984. Sediment Transport, Part II: Suspended Load Transport. Journal of Hydraulic Engineering, 110(11), pp. 1613-1641

Winterwerp, JC, and WGM van Kesteren, 2004. Introduction to the physics of cohesive sediments in the marine environment. Developments in Sedimentology, 56. Elsevier.

Winterwerp, JC 2005. Equilibrium and non-equilibrium floc sizes - or: flocculation takes time. In: IG Droppo, GG Leppard, TG Milligan. Flocculation in Natural and Engineered Environmental Systems, CRC Press, pp 249-270

Wall GR, EA Nystrom, and S Litten, 2006. Use of an ADCP to Compute Suspended-Sediment Discharge in the Tidal Hudson River, New York. USGS SIR 2006-5055.

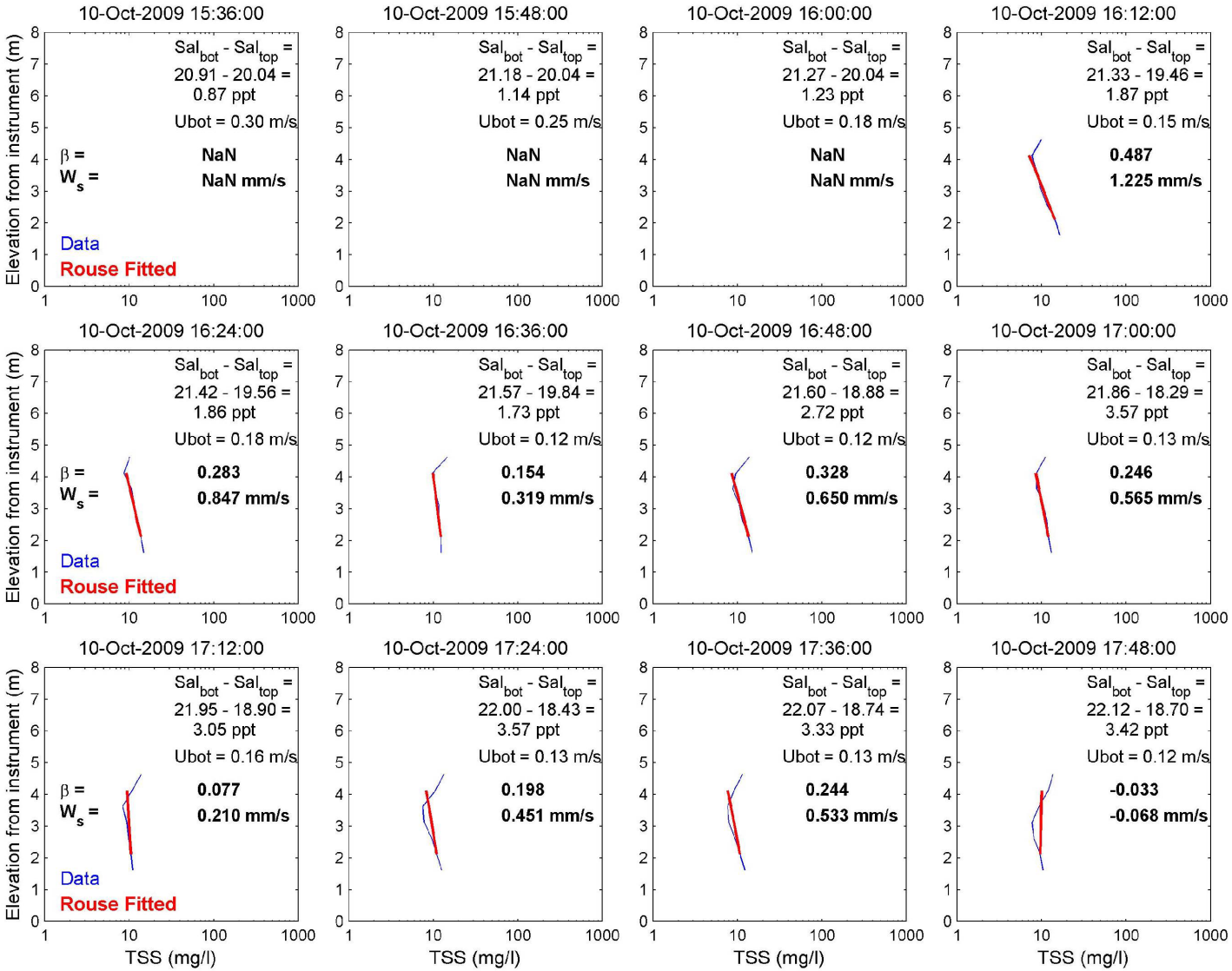


Figure 1. Example profiles of vertical SSC-distribution and Rouse fit; RM 1.4 (PWCM data).

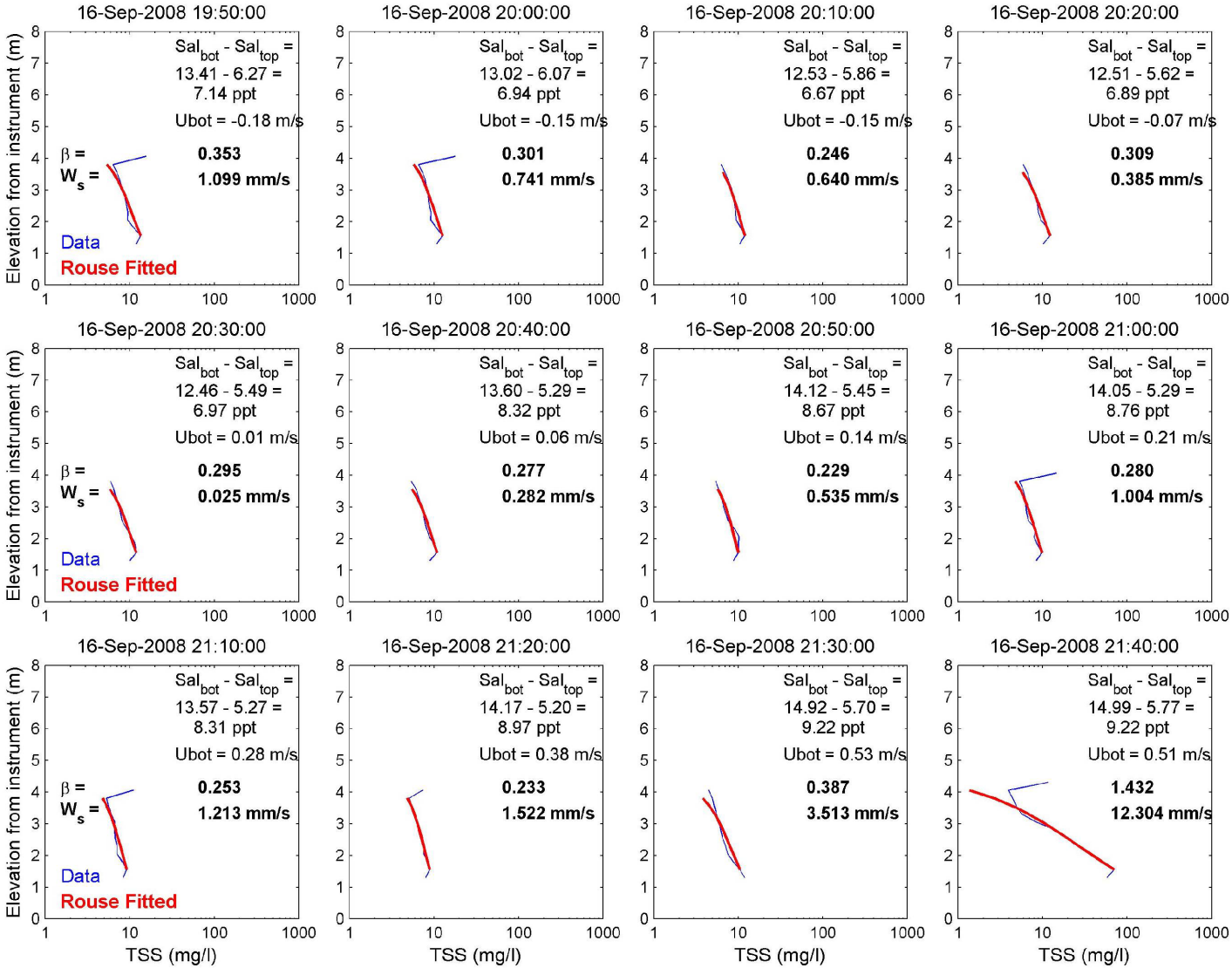


Figure 2. Example profiles of vertical SSC-distribution and Rouse fit; RM 1.4 (Chant data).

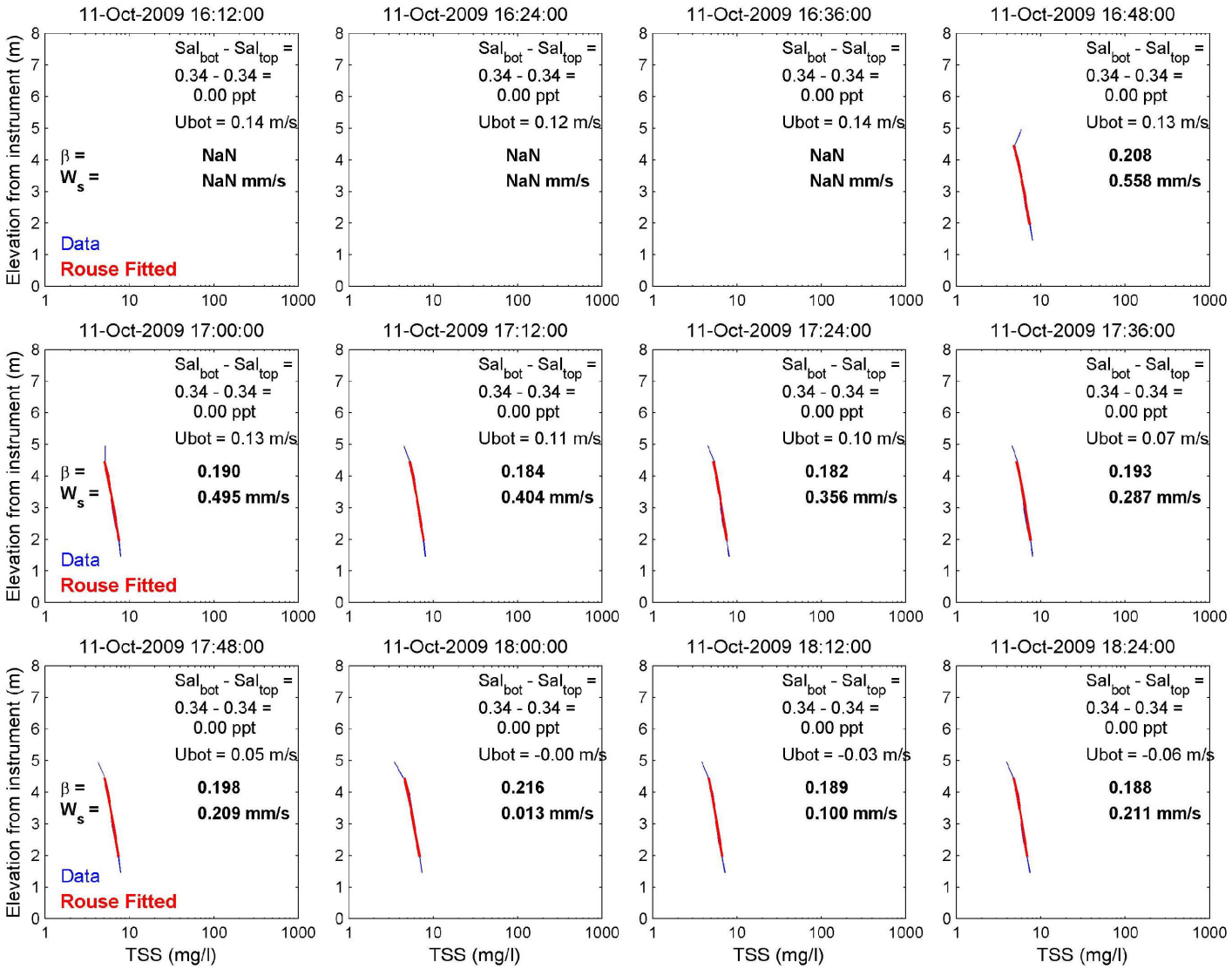


Figure 3. Example profiles of vertical SSC-distribution and Rouse fit; RM 13.5 (PWCM data).

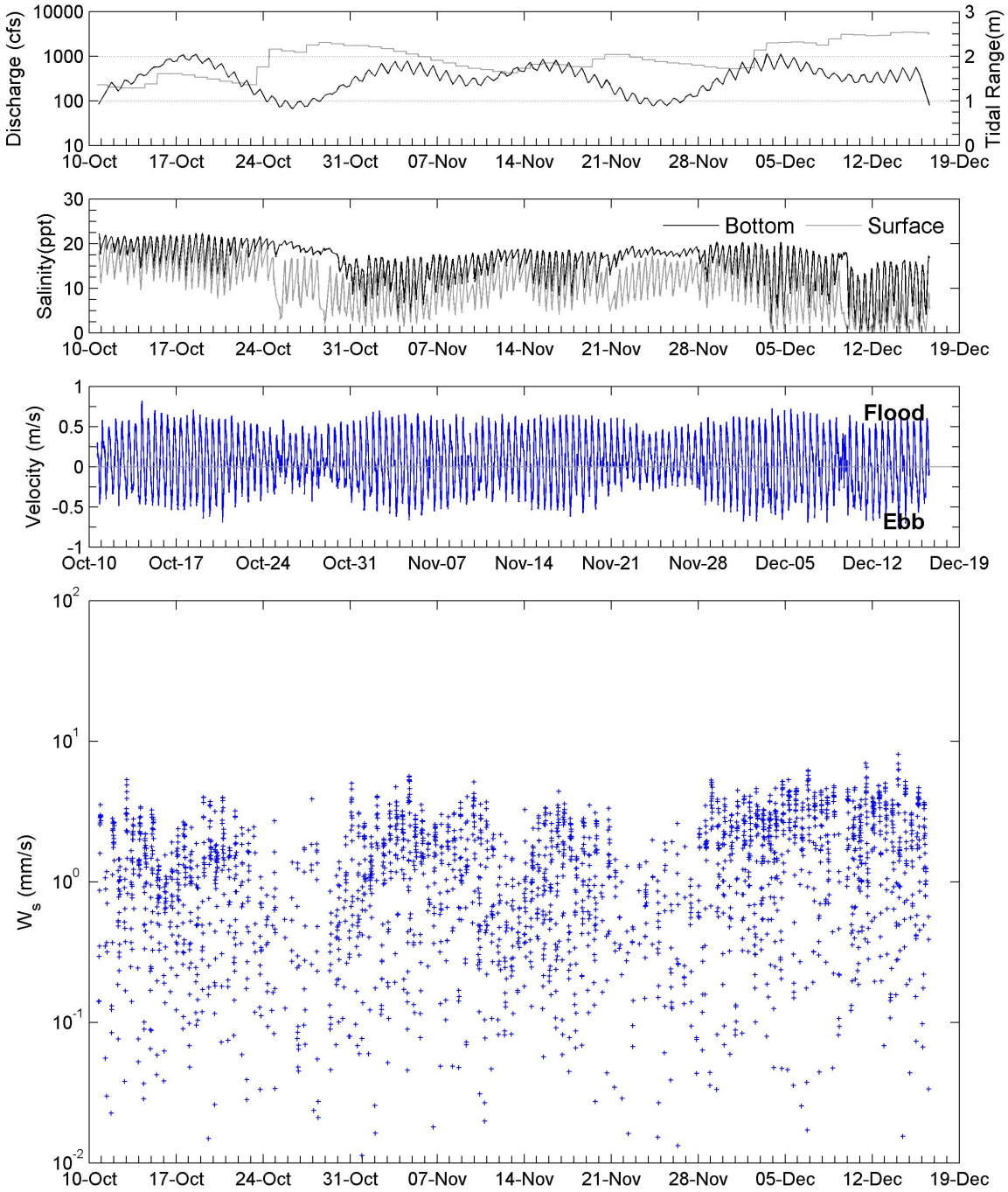


Figure 4. Time series settling velocity and ambient parameters, RM 1.4 (PWCM data)

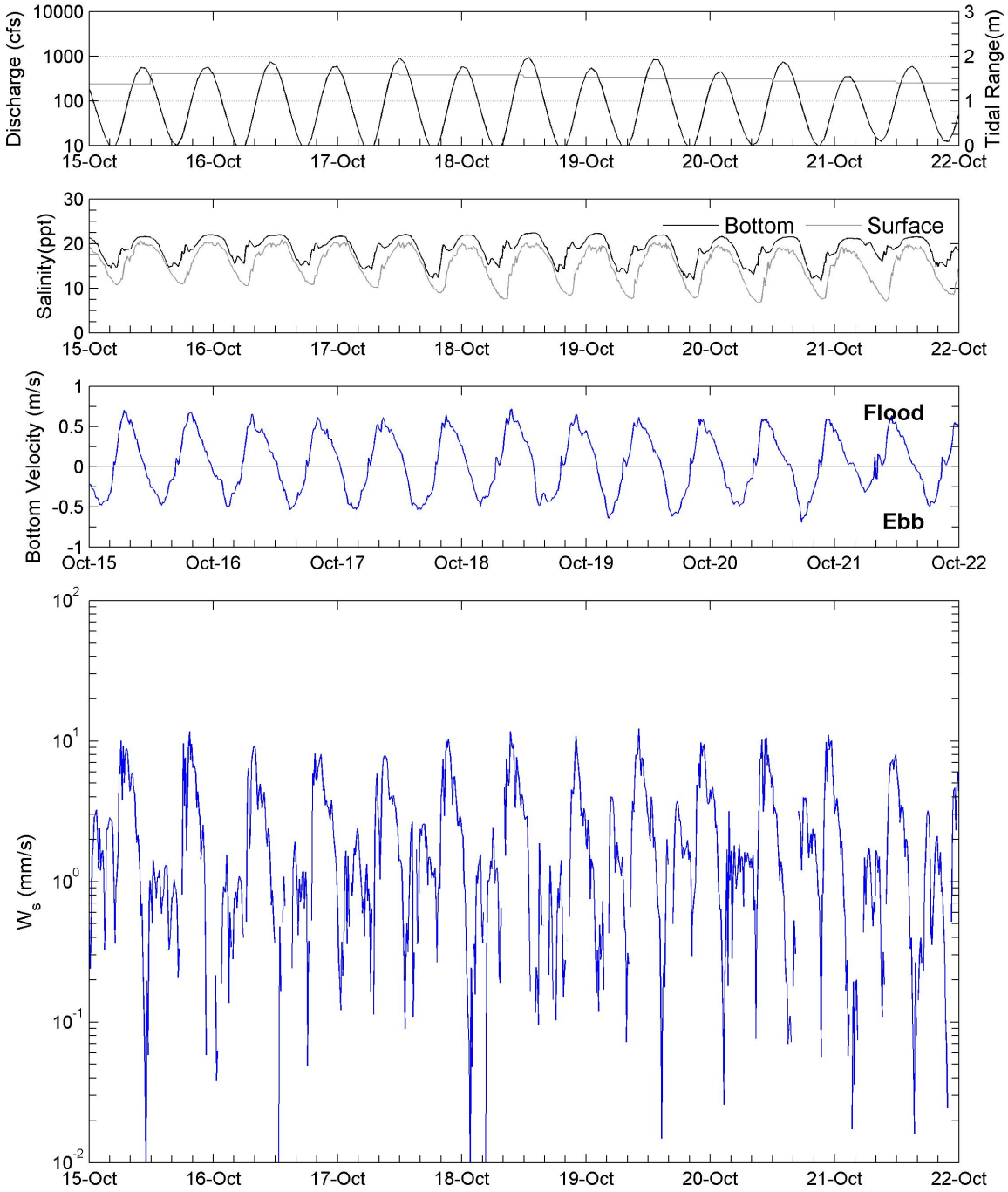


Figure 5. Short-term time series settling velocity and ambient parameters, RM 1.4 (PWCM data)

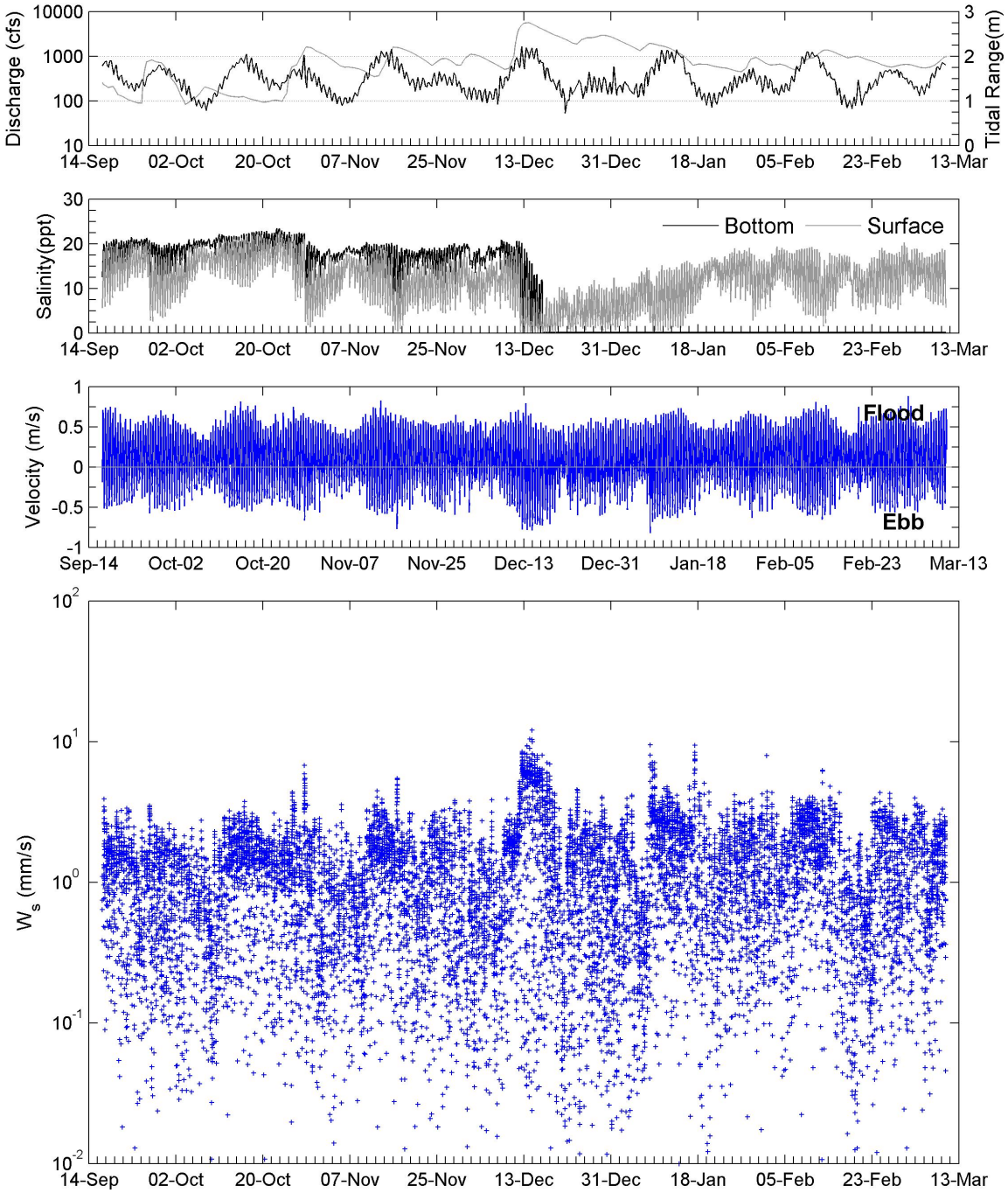


Figure 6. Time series settling velocity and ambient parameters, RM 1.4 (Chant-data)

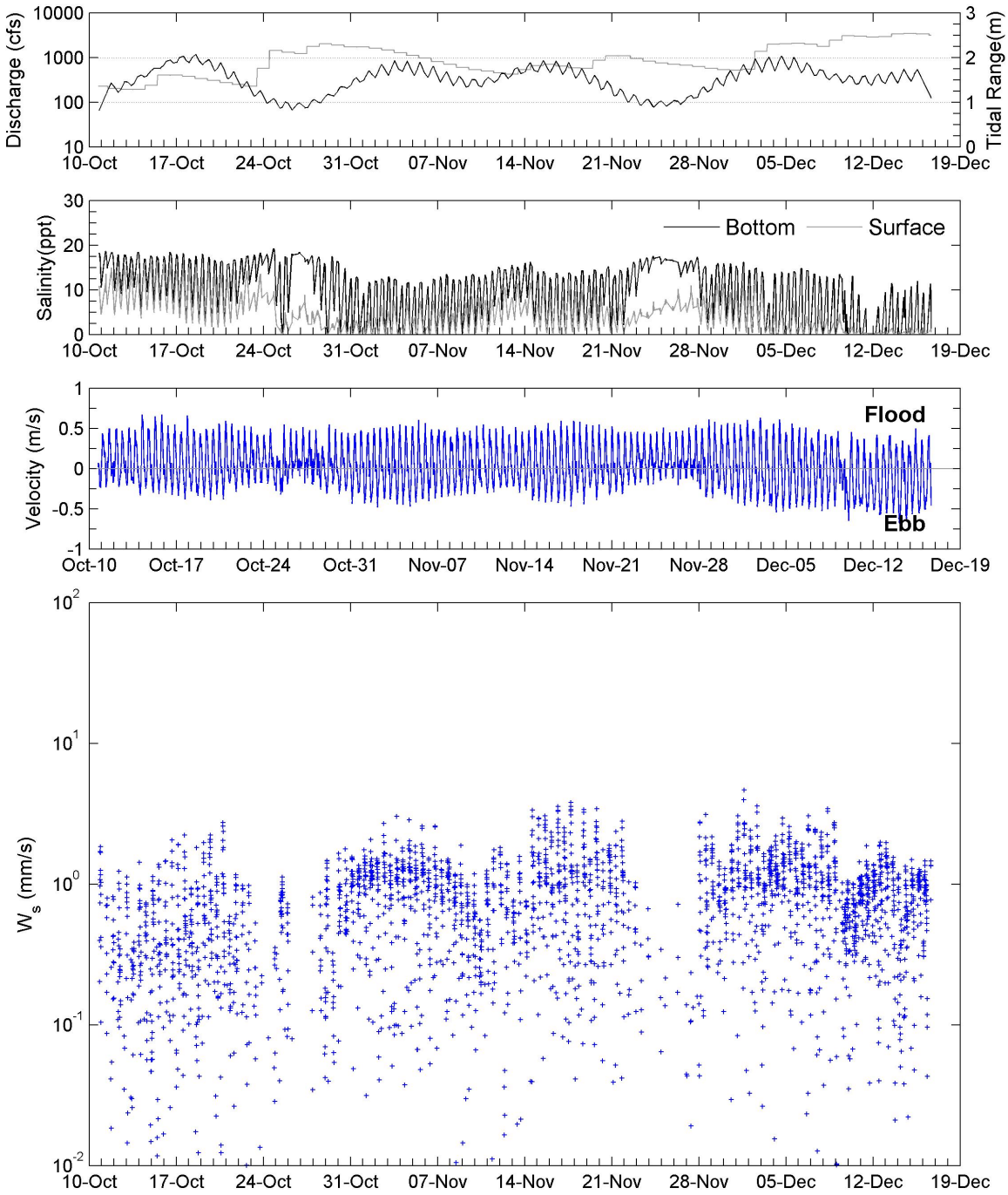


Figure 7. Time series settling velocity and ambient parameters, RM 4.2 (PWCM data)

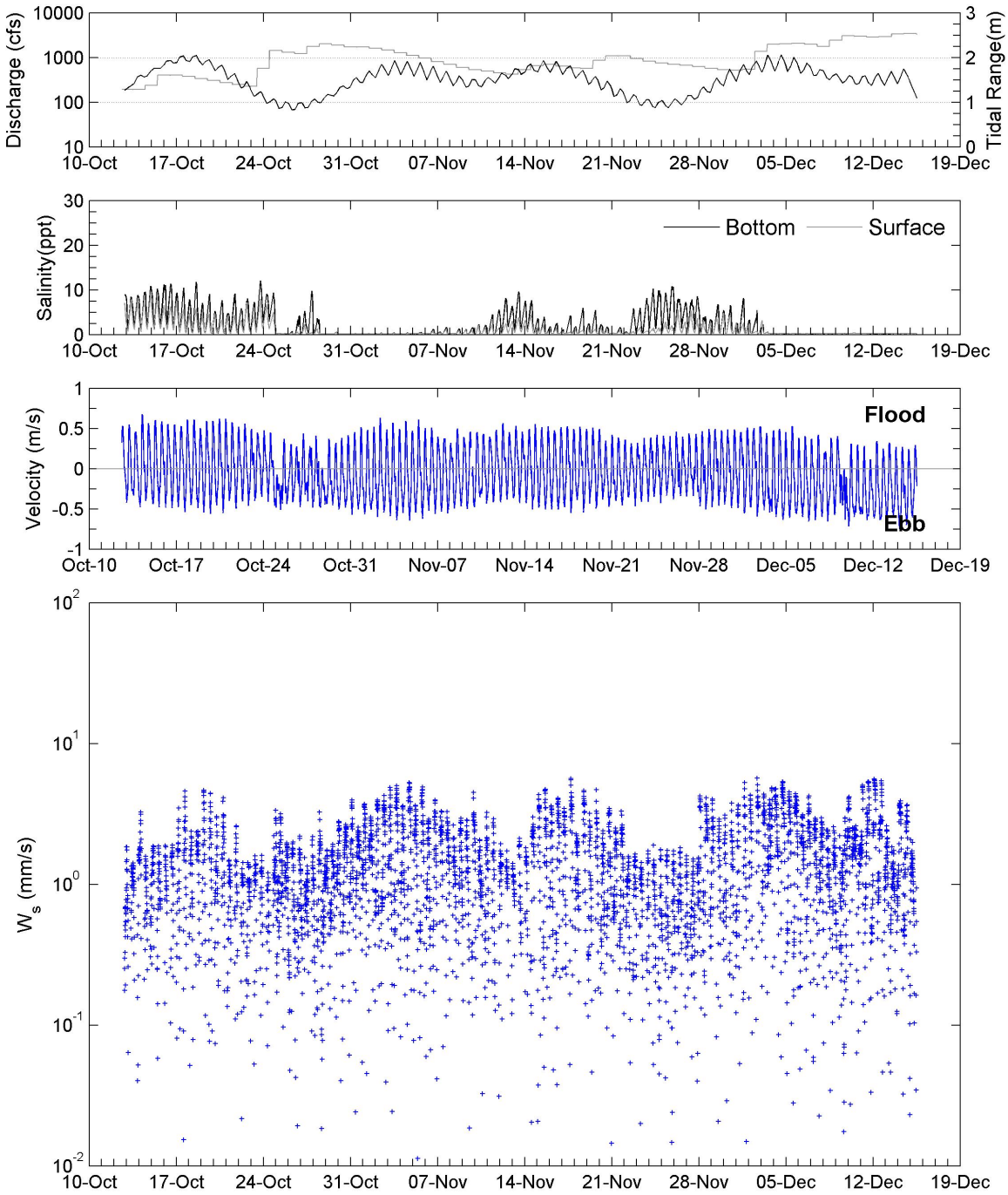


Figure 8. Time series settling velocity and ambient parameters, RM 6.7 (PWCM data)

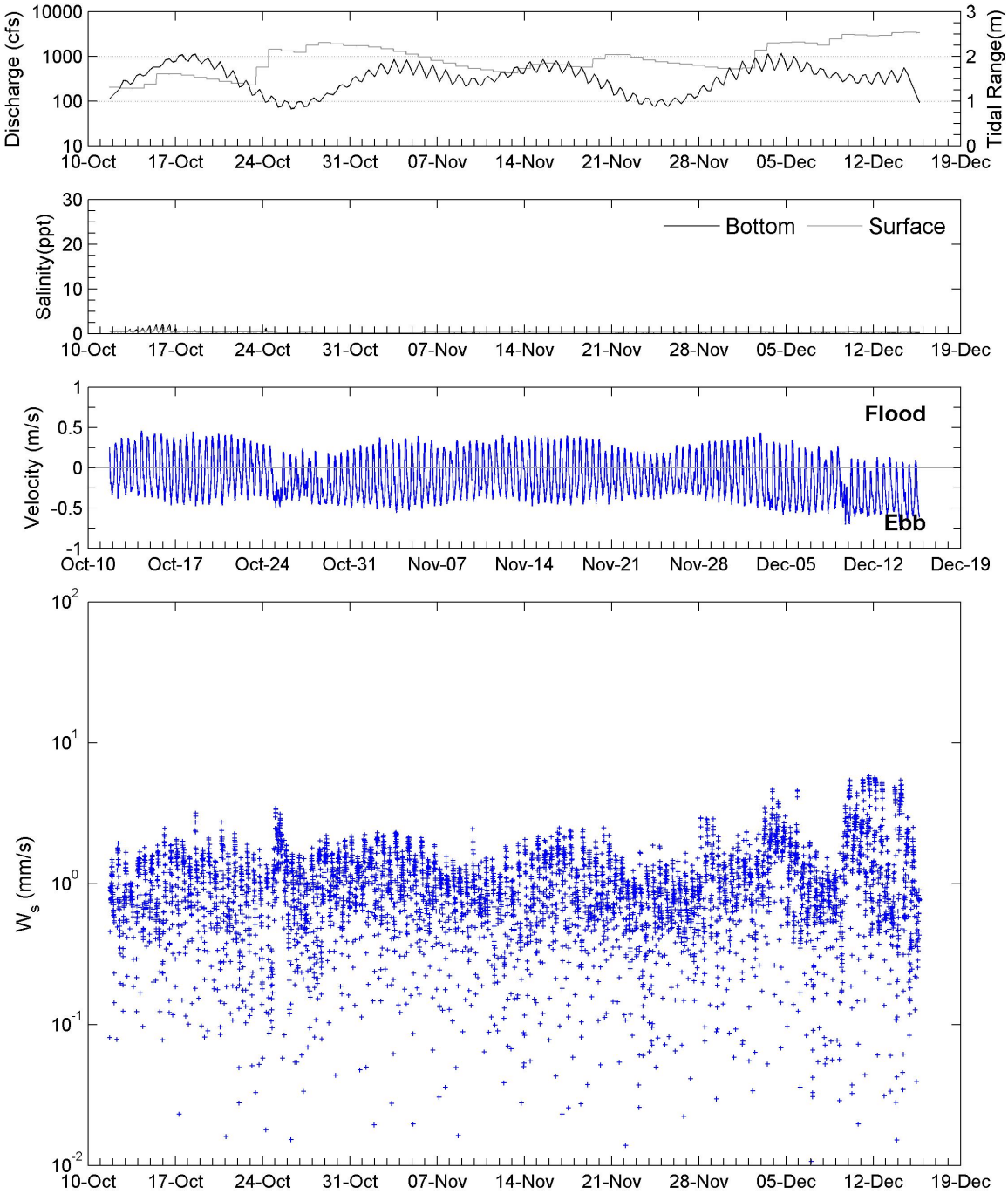


Figure 9. Time series settling velocity and ambient parameters, RM 10.2 (PWCM data)

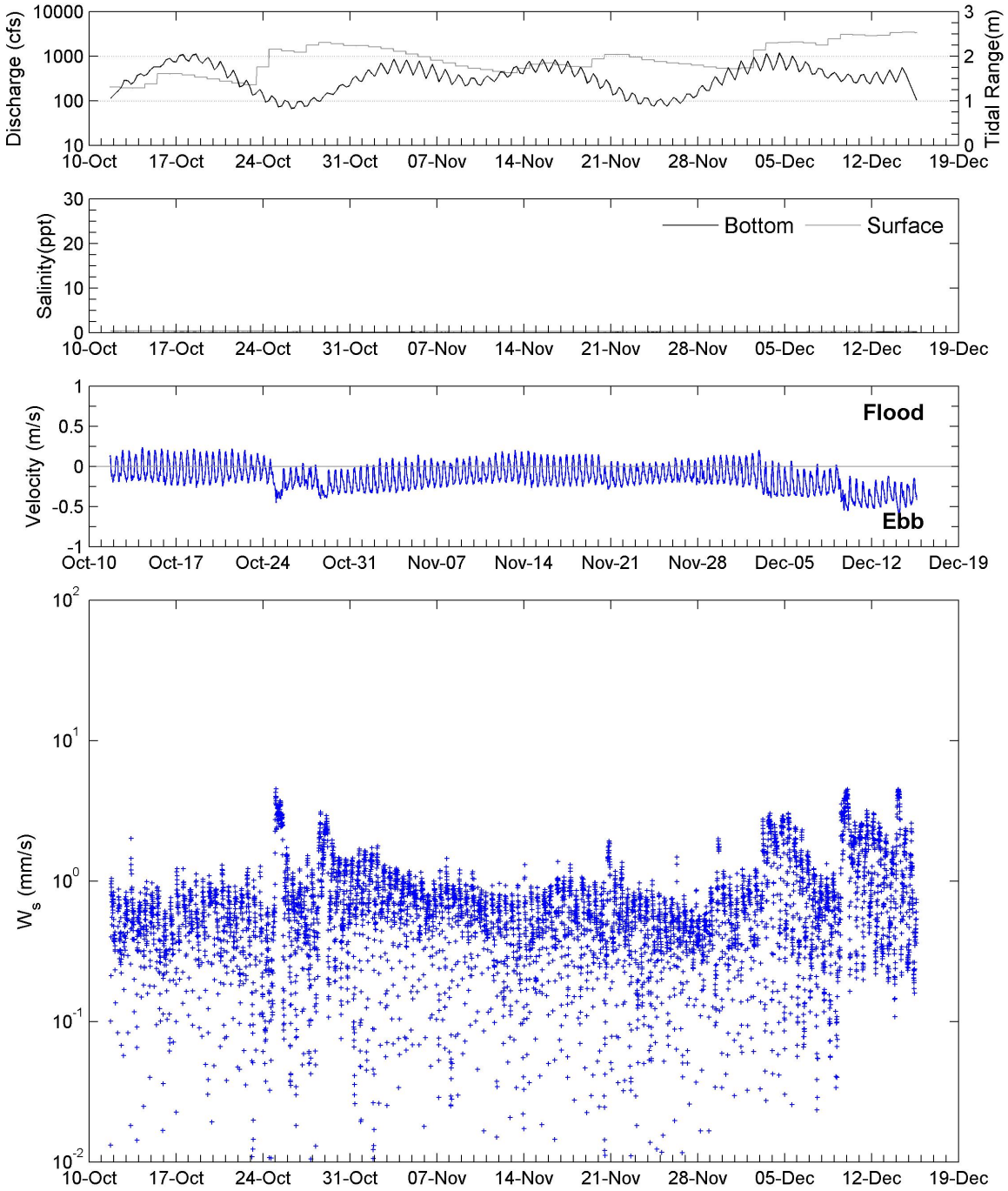


Figure 10. Time series settling velocity and ambient parameters, RM 13.5 (PWCM data)

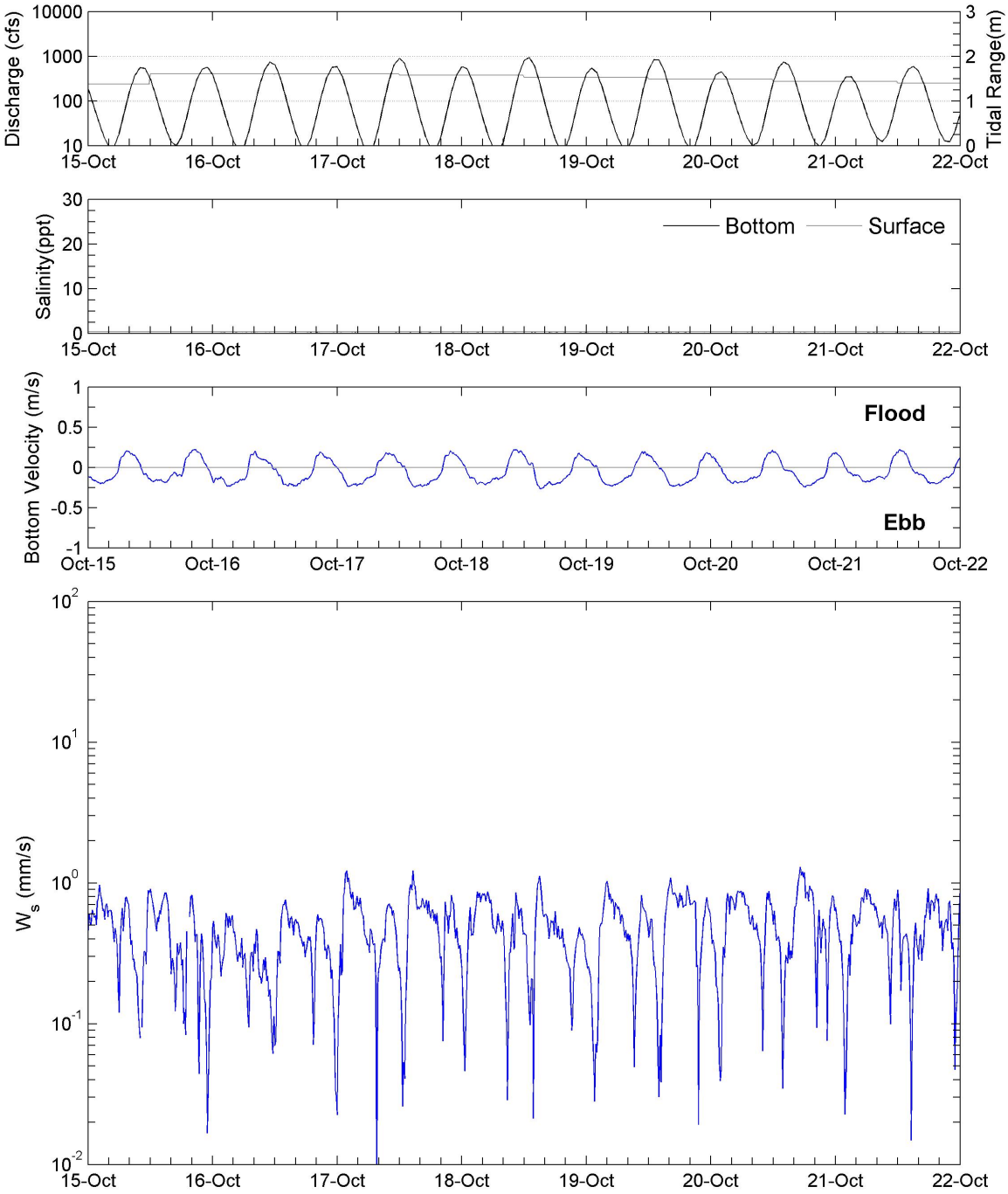


Figure 11. Short-term time series settling velocity and ambient parameters, RM 13.5 (PWCM data)

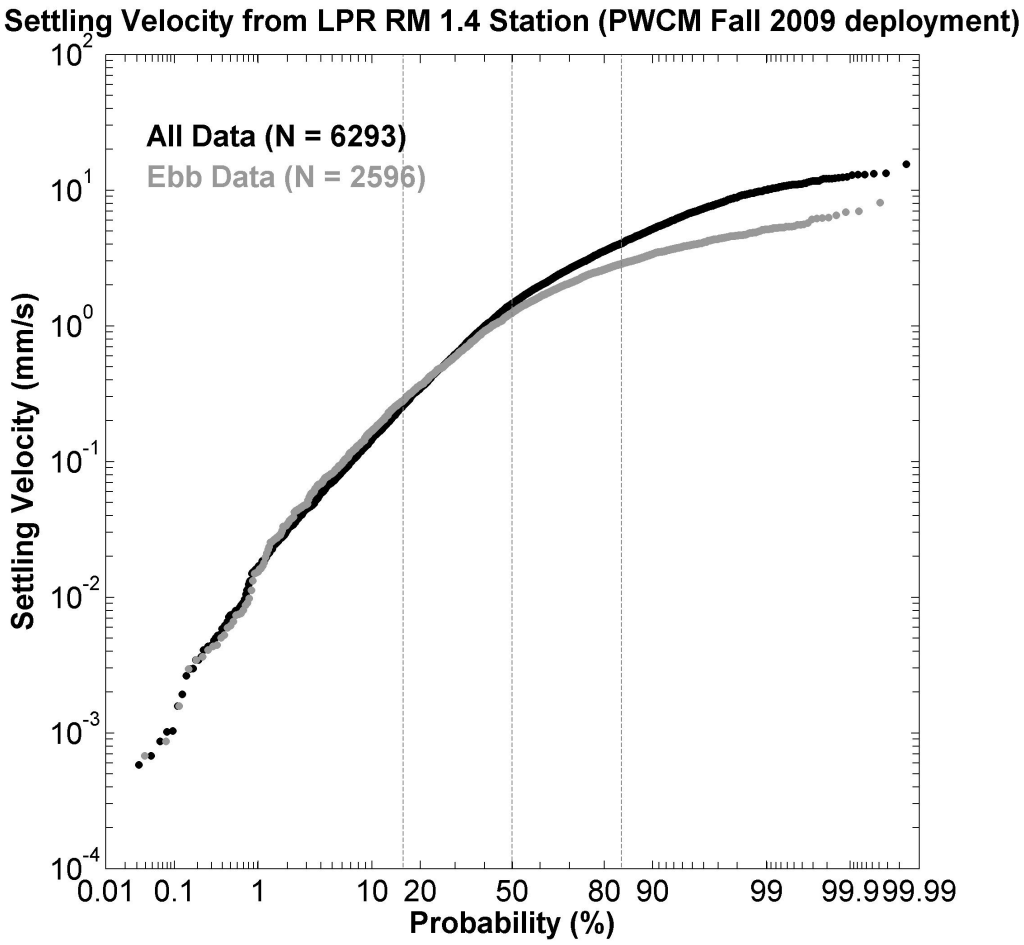


Figure 12. Settling velocity distribution RM 1.4 (PWCM data)

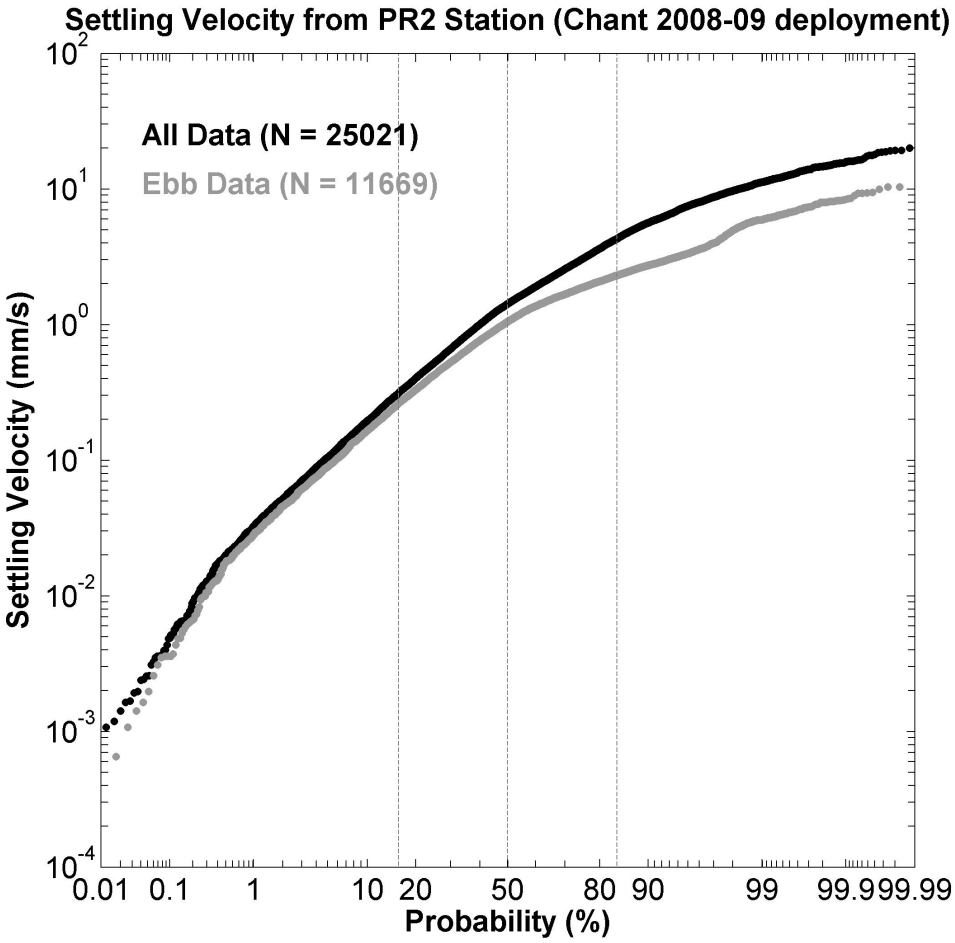


Figure 13. Settling velocity distribution RM 1.4 (Chant data)

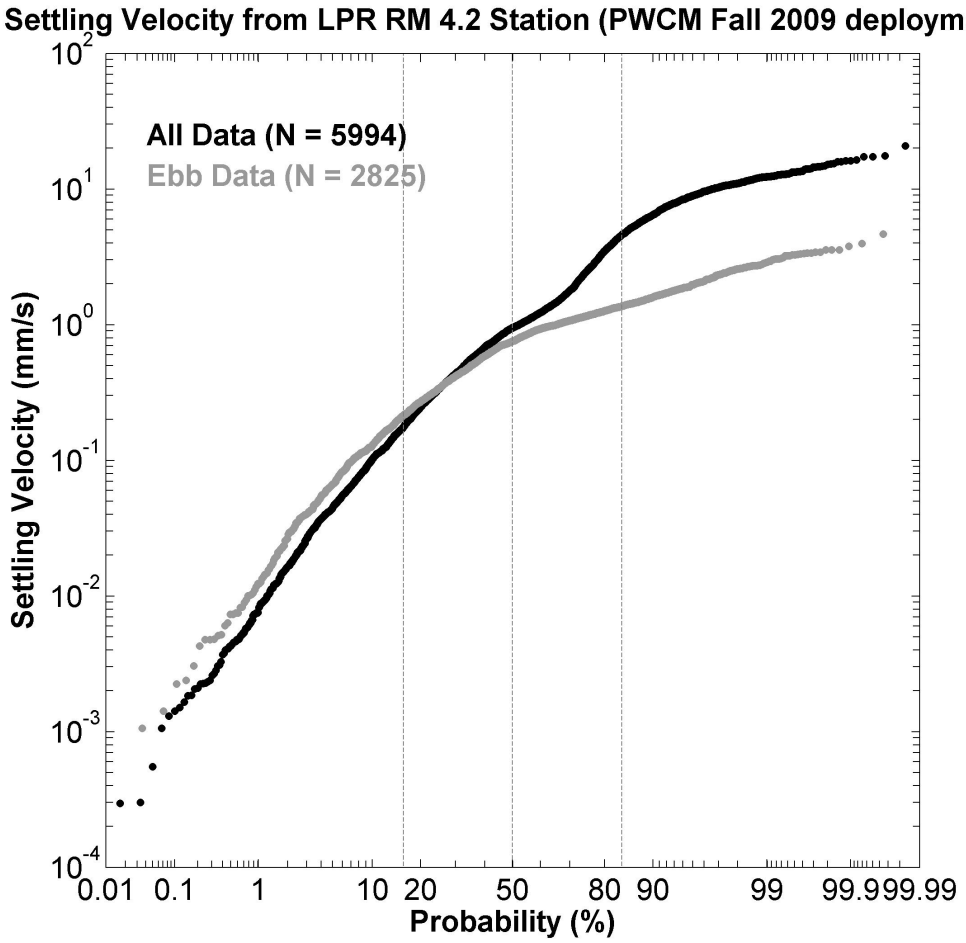


Figure 14. Settling velocity distribution RM 4.2 (PWCM data)

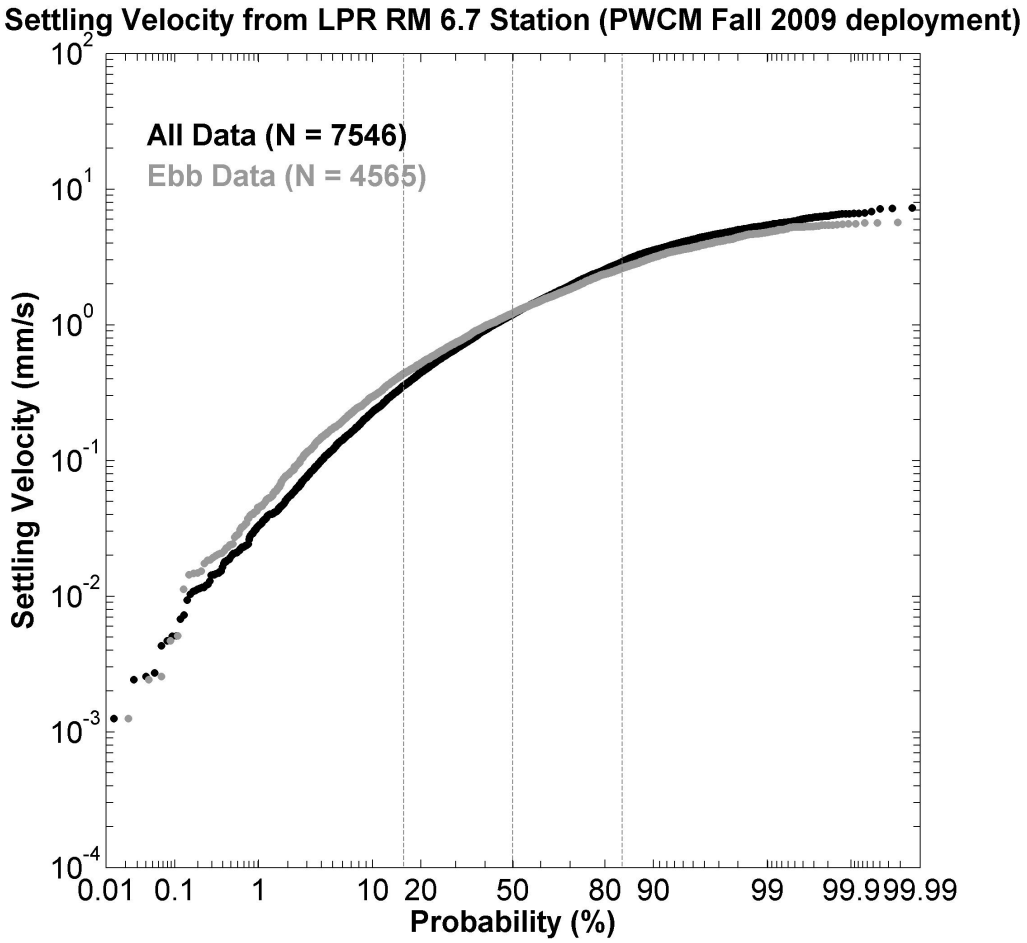


Figure 15. Settling velocity distribution RM 6.7 (PWCM data)

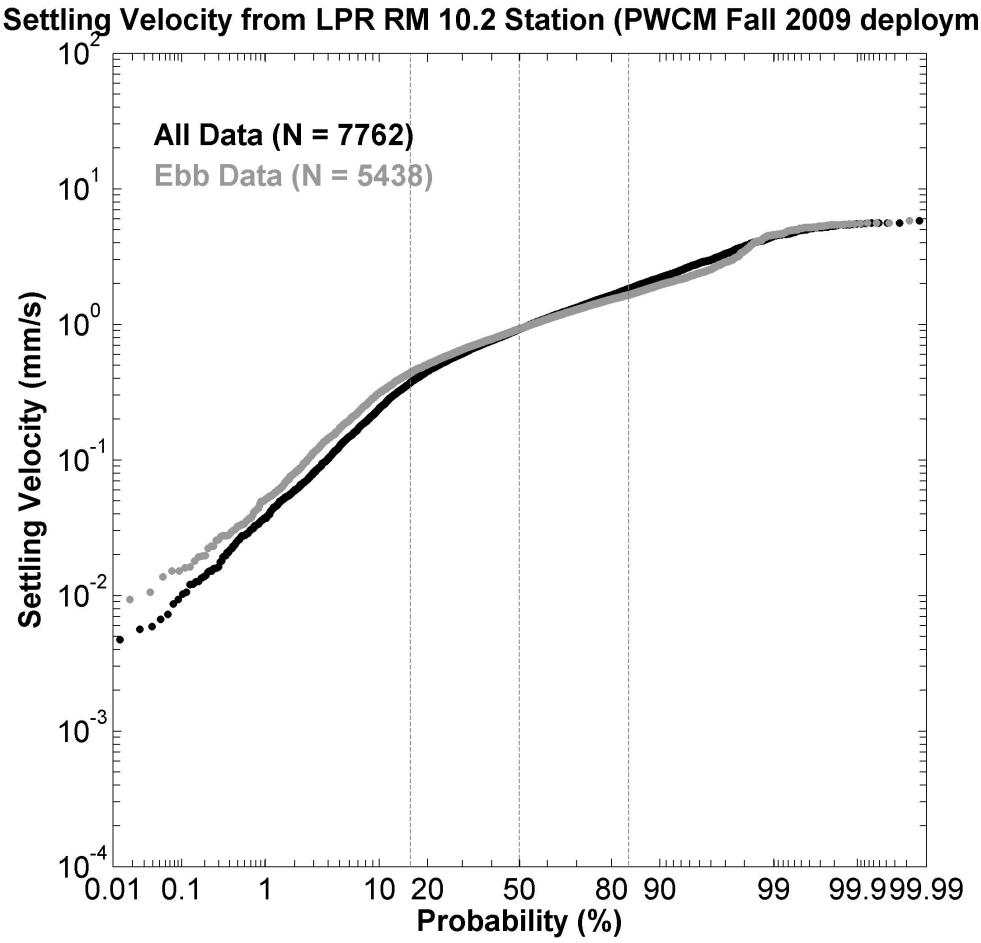


Figure 16. Settling velocity distribution RM 10.2 (PWCM data)

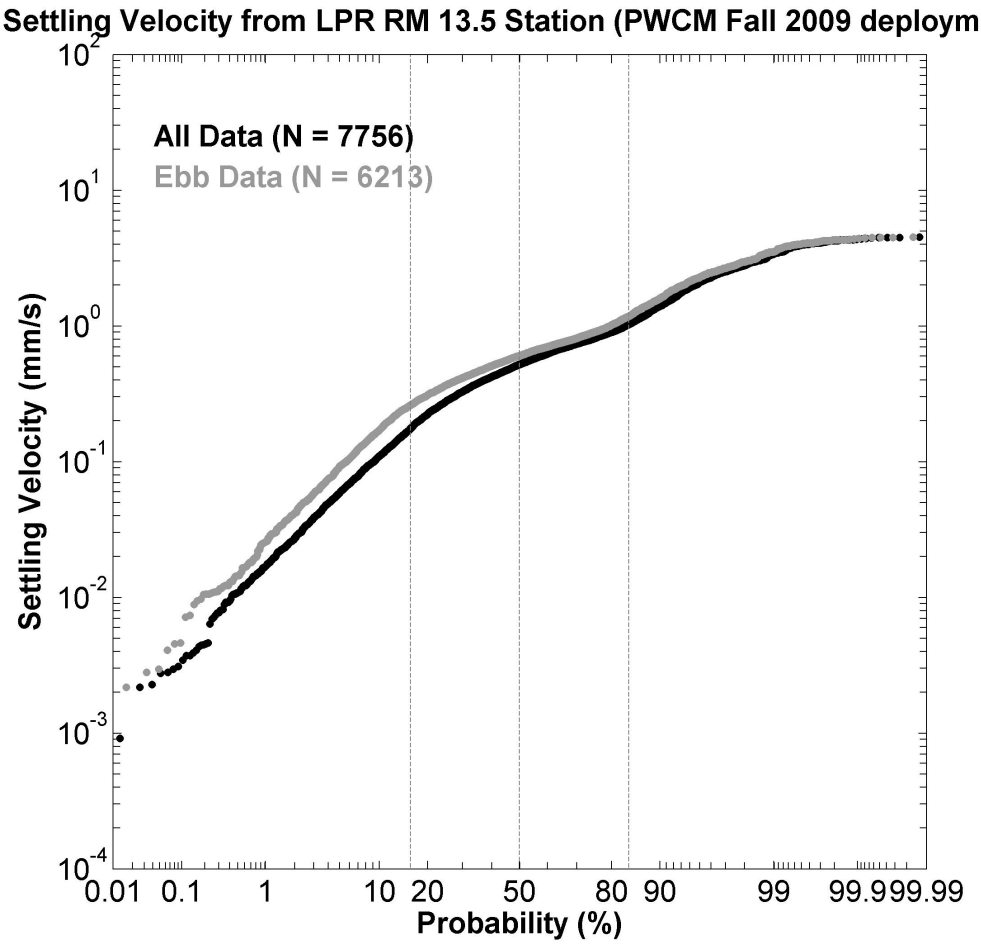


Figure 17. Settling velocity distribution RM 13.5 (PWCM data)

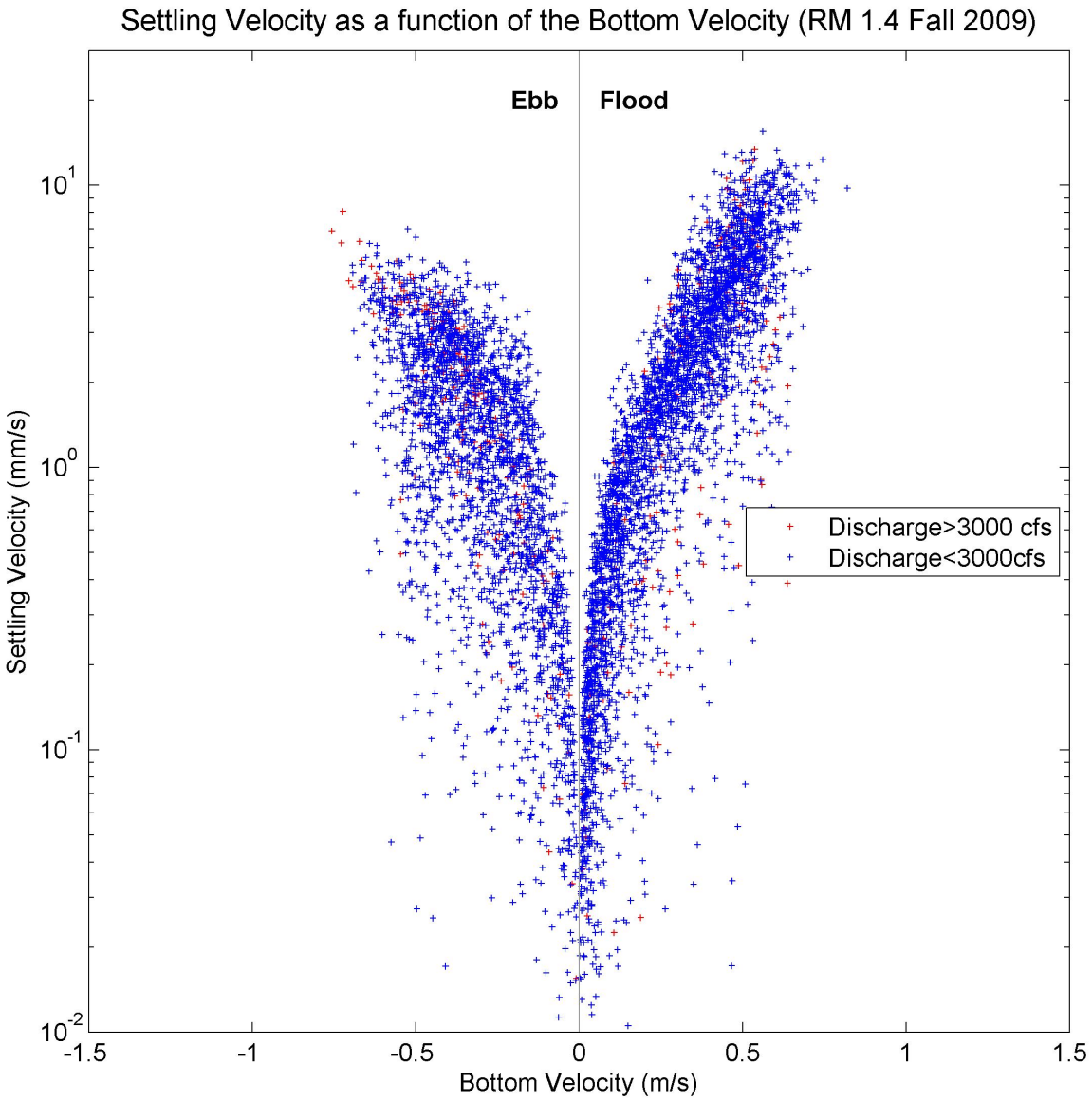


Figure 18. Relation between settling velocity and near-bed flow velocity, RM 1.4 (PWCM data)

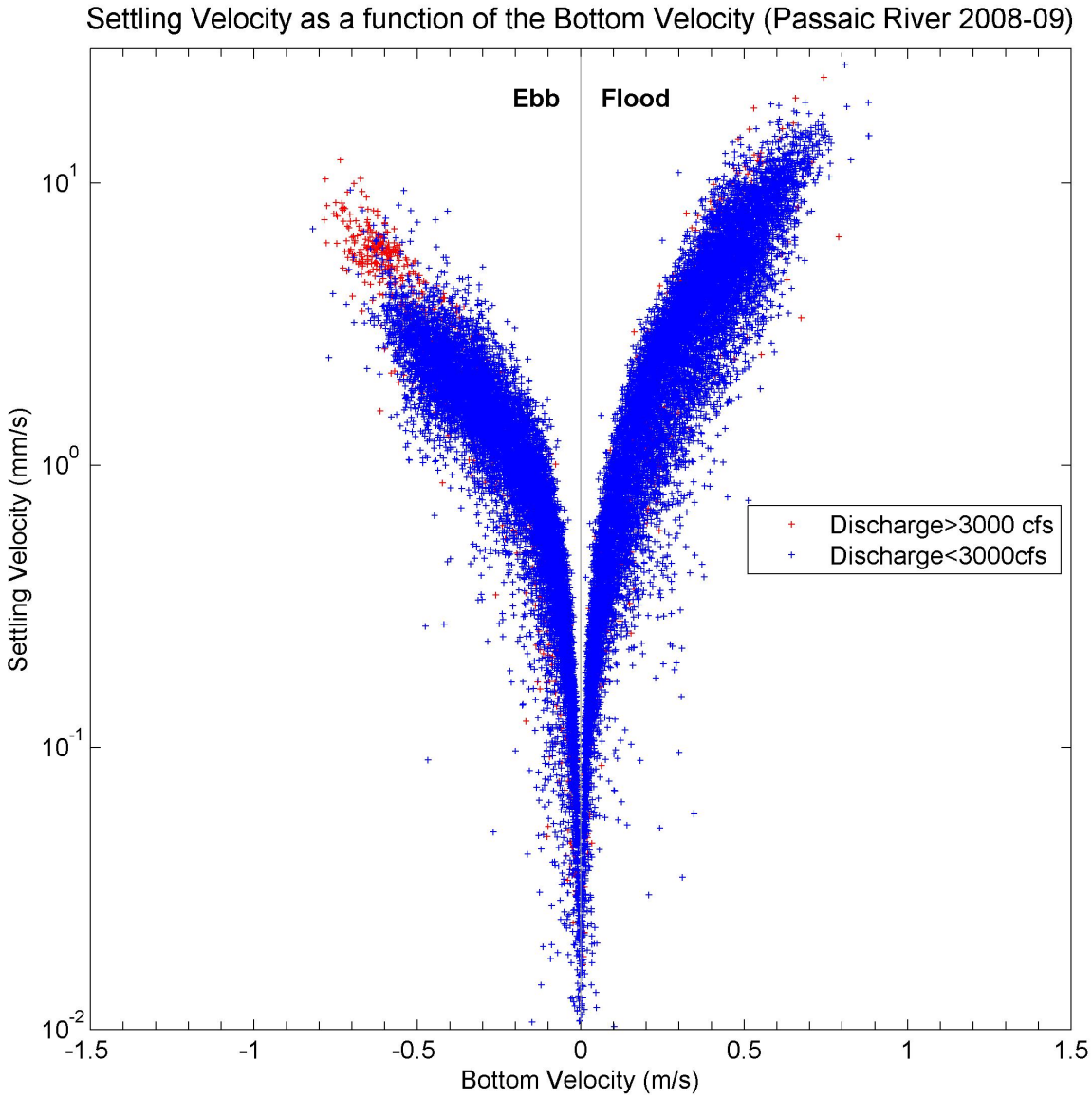


Figure 19. Relation between settling velocity and near-bed flow velocity, RM 1.4 (Chant data)

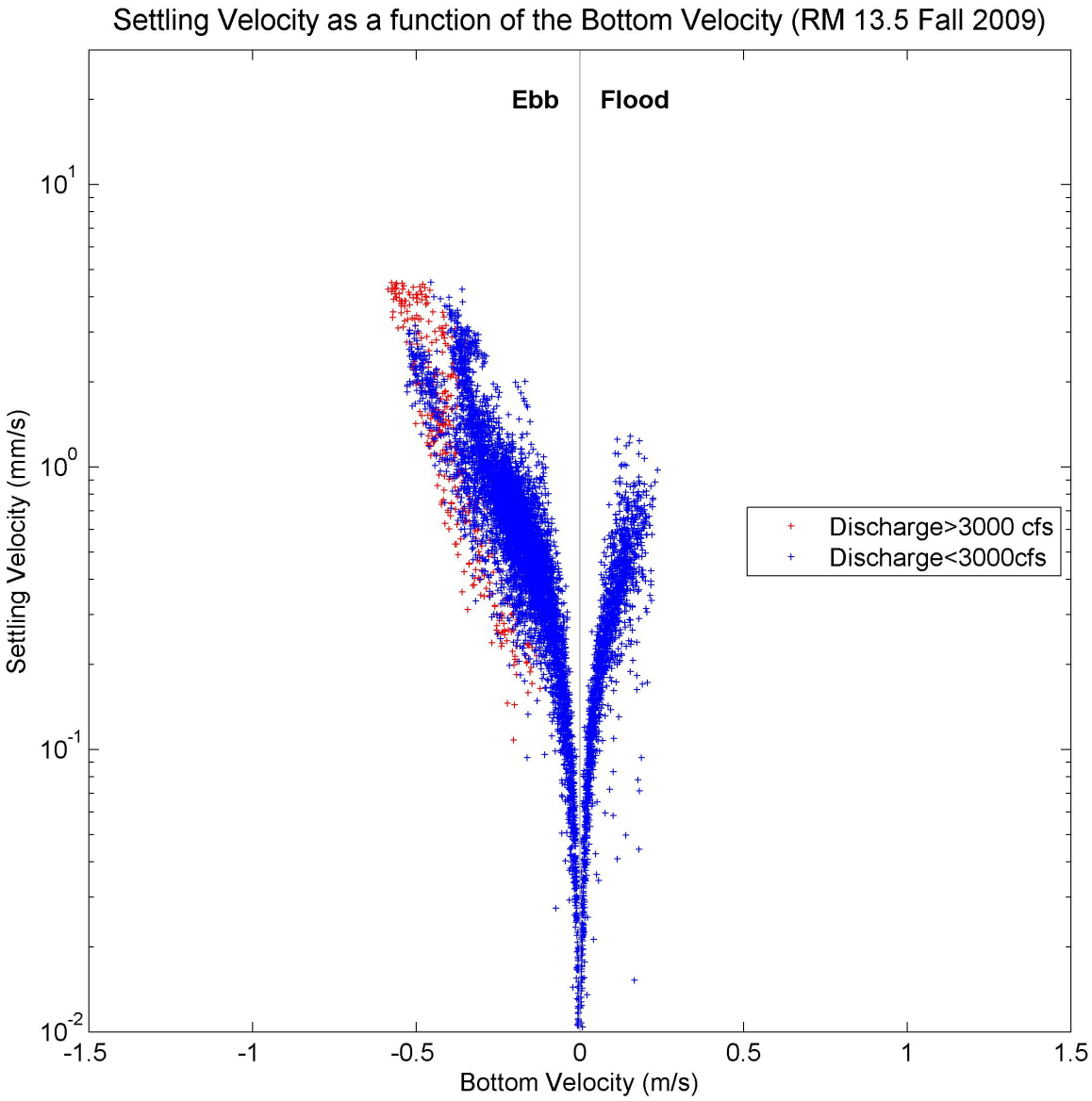


Figure 20. Relation between settling velocity and near-bed flow velocity, RM 13.5 (PWCM data)

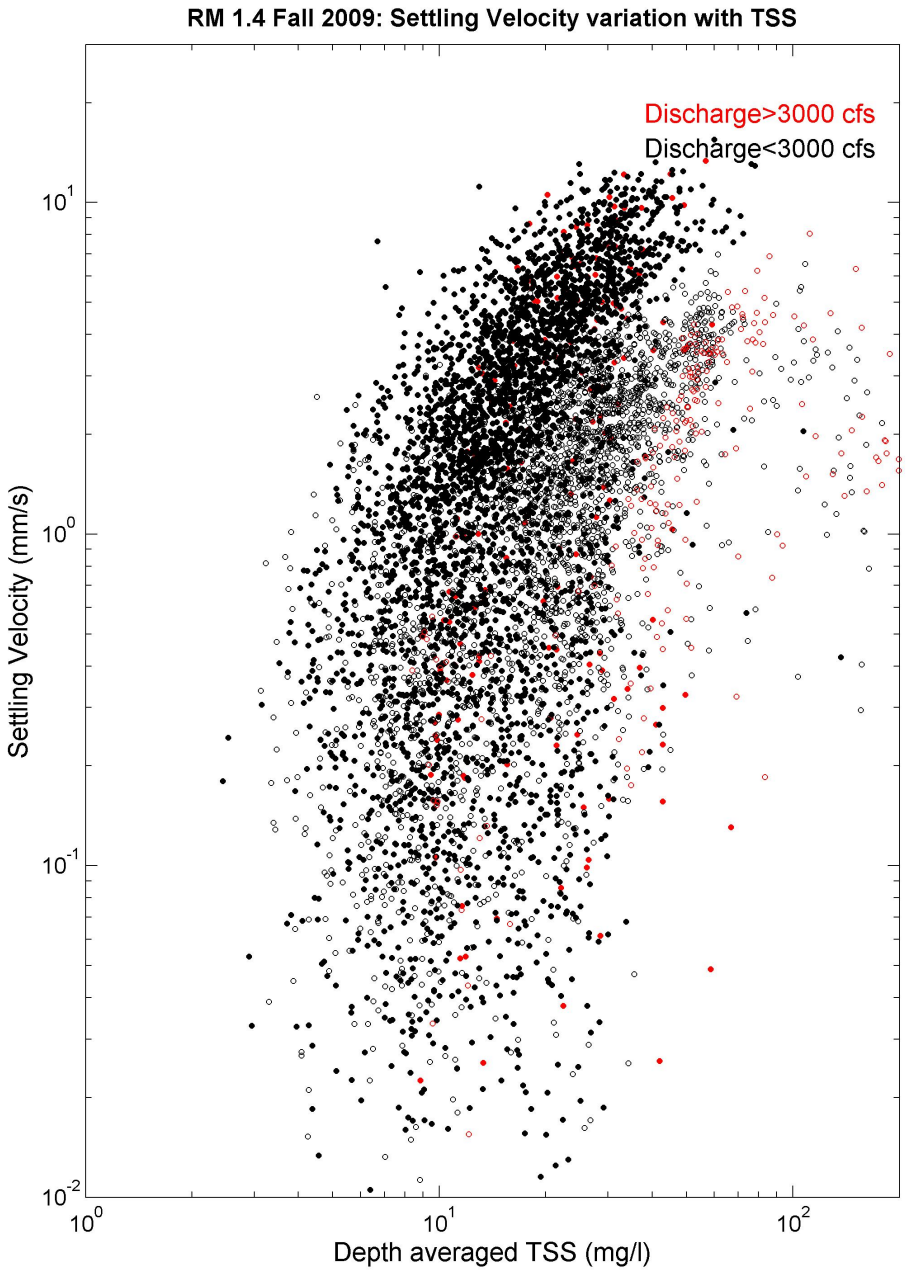


Figure 21. Relation between settling velocity and total suspended solids, RM 1.4 (PWCM data)

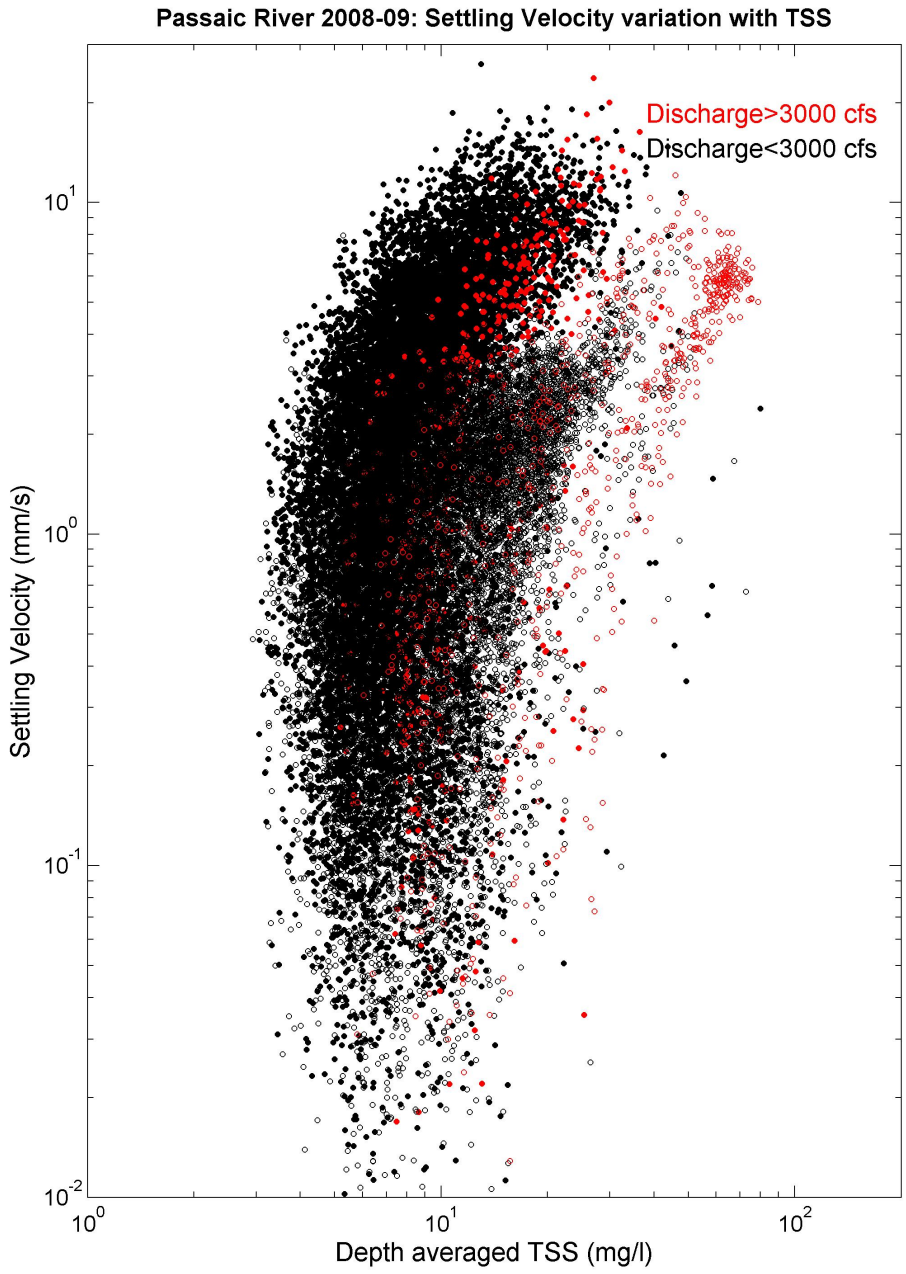


Figure 22. Relation between settling velocity and total suspended solids, RM 1.4 (Chant data)

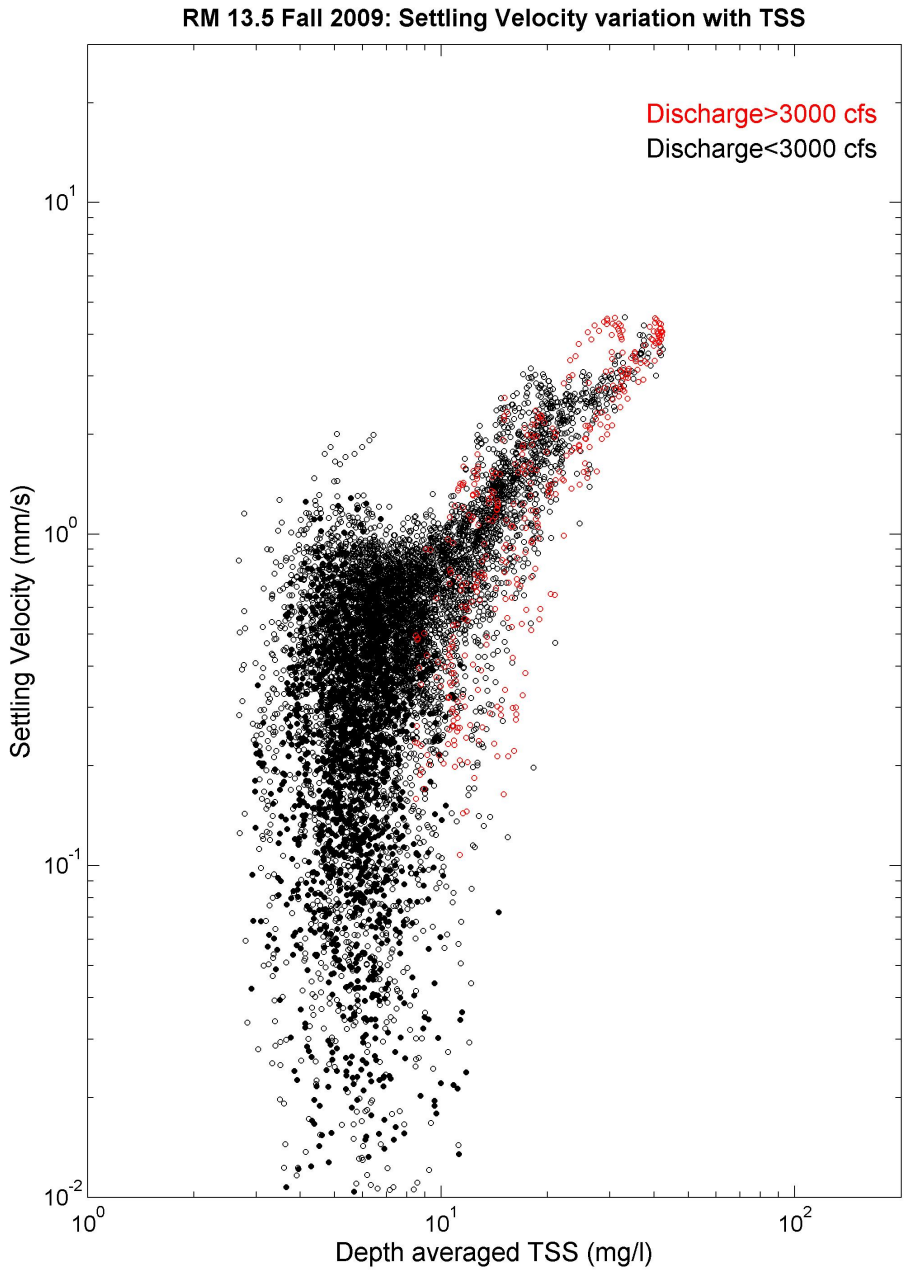


Figure 23. Relation between settling velocity and total suspended solids, RM 13.5 (CPG data)

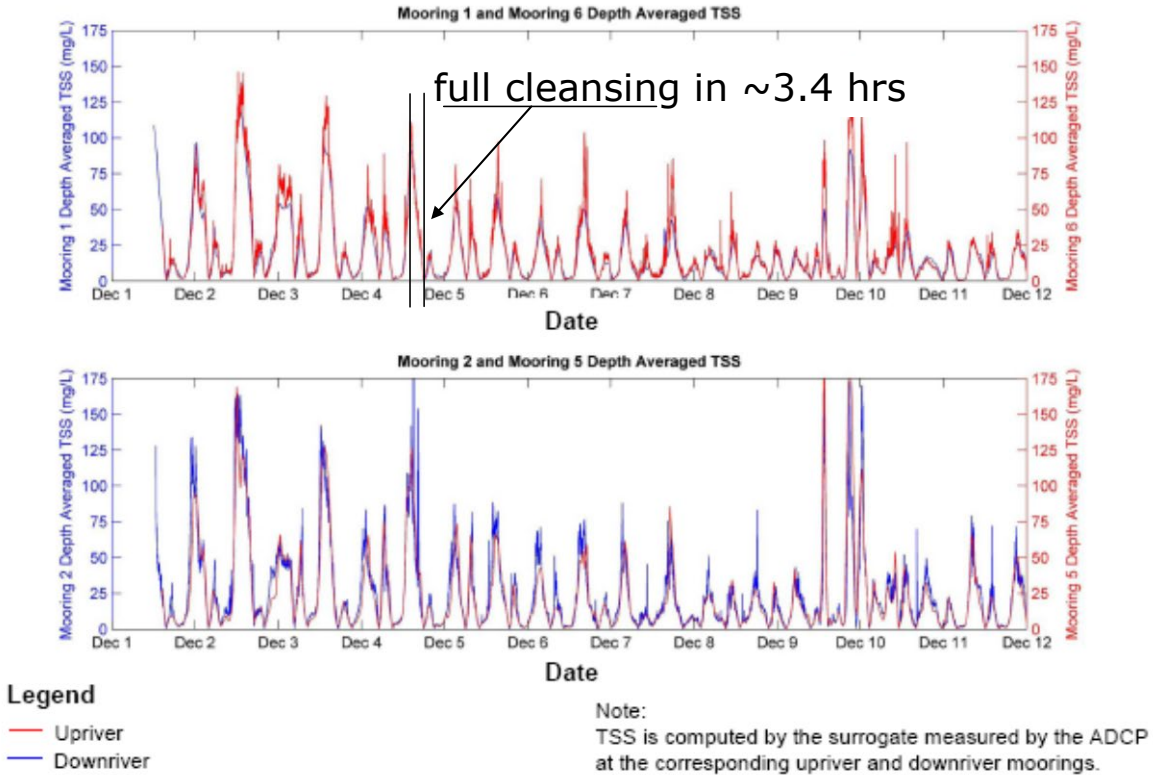


Figure 24. SSC measurements during Pilot Dredging experiment

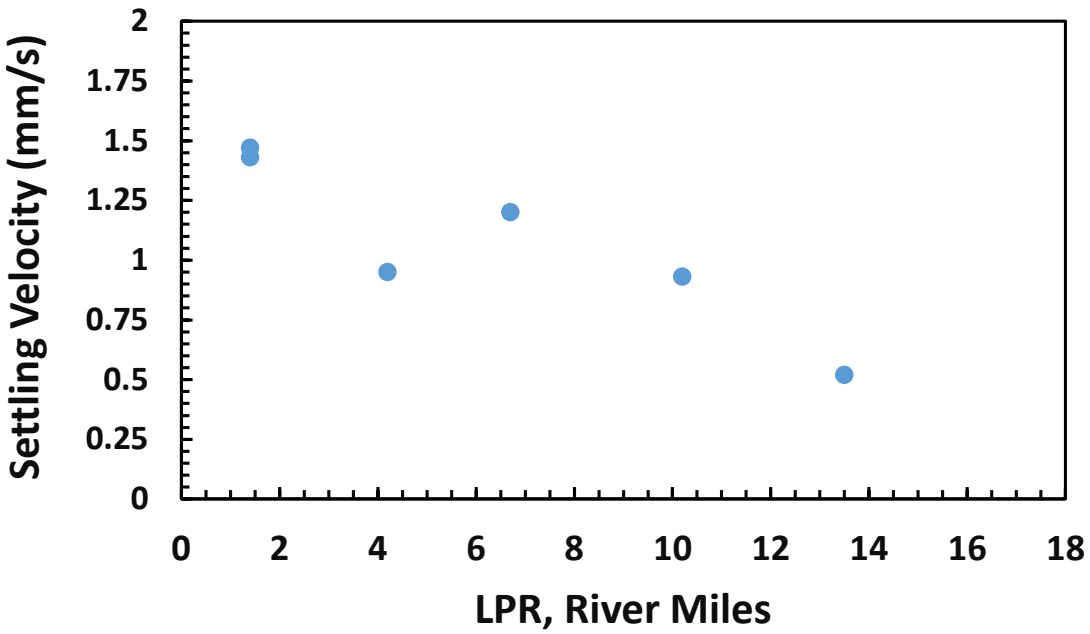


Figure 25. Variation of median settling velocity along Lower Passaic River.